BioCore Exploring Scientific Community

International Journal of Biotechnology and Bioengineering

Research Article ISSN 2475-3432

# Characterization of Air Plasma sprayed Al $PO_4$ and Laser Sealed $Zro_2$- Mgo Coatings on Ni-Base Supper Alloys of Aero Engine

**Khalid. Fared Ahmed***

*Buraydah Private Colleges Qasim Arabic Kingdom of Saudi Arabia*

## Abstract

Aerospace gas turbine engines are now designed such that the heat resistant super alloys operate at temperature very close to their melting, so current strategies for performance improvement are centered on thermal barrier coatings. Lower thermal conductivities lead to temperature reductions at the substrate/bond coat interface which slows the rate of the thermally induced failure mechanisms. Alternatively, lower thermal conductivity of thermal barrier coating (TBC) layers might allow designers to reduce the TBC thickness there by decreasing the significant centrifugal load that the mass of the TBC imposes on the rotating turbine engine components. One approach to improve TBC system is to optimize the pore morphologies in order to reduce the thermal conductivity while still retaining high in-plane compliance. The second approach to improve TBC system performance is to optimize the surface microstructure, surface densification, phase structures mechanical characteristic, chemical structure, and thermo-physical properties. The main focus of this work is to study the influence of AL $PO_4$ (and laser)-sealed $ZrO_2$-MgO coatings on thermal barrier coating system comprised of zirconia stabilized with magnesia top coat to predict the best improvement of TBC system and to optimize the surface microstructure, surface densification, phase structures, mechanical characteristic, chemical structure, and thermo-physical properties as well as their properties with those obtained using reference techniques. Thermal expansion studies were used to study the high temperature stability of the different coatings (reference and modified coatings) structures. As low thermal conductivity is one of the most important features of TBC, thermal diffusivity and specific heat measurements were carried out. Also the mechanical measurements (e.g. micro-hardness, tensile bond strength, young's modulus), phase analyses using XRD and chemical analysis using electron dispersive X-ray (EDX) for elemental analysis in scanning microscopy studies

**Keywords:** Thermal Barrier Coating, Air Plasma Spray, Heat Treatment, Thermal Expansion Coefficient, Thermal Conductivity, Zirconia Stabilized With Magnesia, Nickel Alumina Coatings, Laser Sealed Zirconia Coatings, Turbine-Engine And Laser Sealed $Zro_2$- Mgo Coatings

**Corresponding author:** **Khalid. Fared Ahmed**

Buraydah Private Colleges Qasim Arabic Kingdom of Saudi Arabia.

**E-mail:** khalidfared330@yahoo.com

**Citation:** Khalid. Fared Ahmed (2018), Characterization of Air Plasma sprayed Al $Po_4$ and Laser Sealed $Zro_2$- Mgo Coatings on Ni-Base Supper Alloys of Aero Engine. Int J Biotech & Bioeng. 4:3, 44-56.



**Received:** March 08, 2018

**Accepted:** March 18, 2018

**Published:** April 07,2018

## Aim and scope of the present work

Aerospace gas turbine engines are designed and operates at temperature very close to their melting points. So current strategies for performance improvements are centered on (thermal barrier coatings) TBCs.

This project was designed to obtain a better understanding of the pore morphologies, the surface microstructure, surface densification, phase structures mechanical characteristic, chemical structure, and thermo-physical properties of ceramic coatings in a high temperature corrosive environment and to help designers of advanced aero, industrial and marine gas turbine engines in the area of TBCs. Whilst in aero engines ceramic coatings are primarily temperatures as a means of increasing life.

## Review

TBCs are often applied to metallic super alloys to extend the temperature regime in which a component can operate [1-6]. A common failure mechanism of TBCs on thermal cycling is delamination of the ceramic just above the bond coat ceramic interface due to high local stresses and that thermal expansion mismatch between the substrate and ceramic layer is a significant contributor to these stresses [7-11] to reduce these stresses three layer system incorporating intermediate layer of graded material between the bond coat and ceramic have been tried while these three layer coating have proved promising for diesel application [12].

Principle Diagram of the Energy Source Shows the different thermal spraying techniques divided by their principle energy sources:

## Plan of work

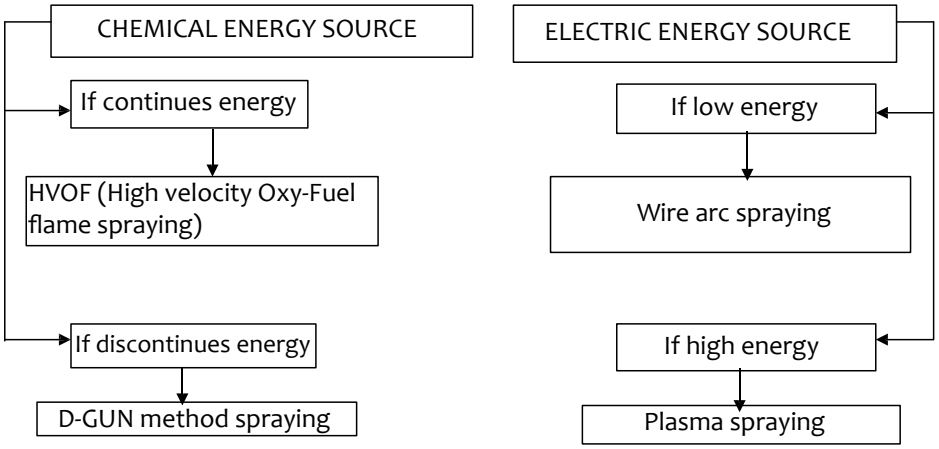


An ideal coating would exhibit a high uniform, well controlled distribution of pores and micro cracks to both decrease thermal conductivity and allow thermal expansion and contraction without exfoliation. At the same time, the coating must be sealed against penetration of corrosive liquids by a high density surface layer. Two approaches, surface densification by heat treatment and impregnation by thermo - chemical methods have been investigated in this work.

## Experimental analysis

PLASMA - TECHNIK AG M - 1000 apparatus for plasma and auxiliary equipment for the spraying of aerospace components. It comprise : powder source (PT - 800), control console (M - 1000), plasma torch (F4), feed unit (TWIN - 10), water cooler system (T -powder 500) and holding device for the work piece in addition to dust separator (MK - 9) and wet separator (NA - 100). Figure (1)., gives a schematic diagram of the apparatus.

Samples cut out of Nickel base super alloy Ni-Cr 20 Ti Al of DIN designation number is corresponding to 2.4631 of 1.4 mm thickness have been subjected to investigations. First, Ni - 5wt % Al (AMDRY, 956) alloy (bond coat) of 0.4 mm to 0.6 mm thickness and then, $Zro_2$ - 20wt % Mg O (AMDRY 333) (top coat) of 0.5 mm to 0.8 mm thickness have been deposited by air plasma spraying method upon their surface.

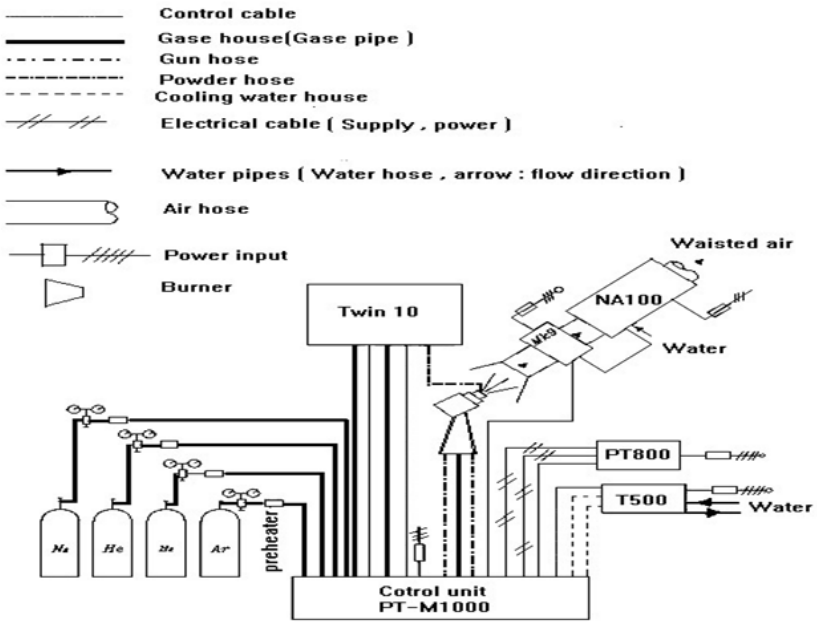


**Figure 1:** Systamatic diagram of plasma spray M- 1000 (plasma - Technik - AG)

### Spraying material investigation

The most important powder parameters are grain size described, in ASTM standard B. 214- 86 using mesh designation number also, in DIN standard DIN 32529 using number to describe the grain size, internal porosity (correlated with apparent density and flow ability described, in ASTM standard B. 329- 76 and B 213- 83. receptivity).

EDX (Electron Diffraction X- ray) was used in chemical analysis.

XRD (X- Ray Diffraction) was used in phase identification and quantitative phase analysis studies.

### Surface investigation

The Vickers Hardness (HV3) was determined using ASTM E- 384 - 73 standard.

The Tensile bond strength measurement using ASTM 633 - 96 or DIN 50160 standard. Porosity were tested with (MIP).

EDX and XRD were used in chemical and phas identification.

The corrosion behavior of specimens was determined using AUTOLAP PGSTAT 30 show in figure (2).

Thermal conductivity, λ, was calculated from thermal diffusivity, α, with laser flash apparatus (Theta Industries Inc., Part Washington, NY, USA), specific heat, cp. With DSC

404 C, and density of the free standing coating specimen.

$$\Lambda = \alpha * Cp * \rho$$

TEC were carried out by dilatometer (Adamel Lhomargy SAS, model DI - 24, France). TCR test was studied in a thermal cycling facility illustrated in figure (3) and table (1).

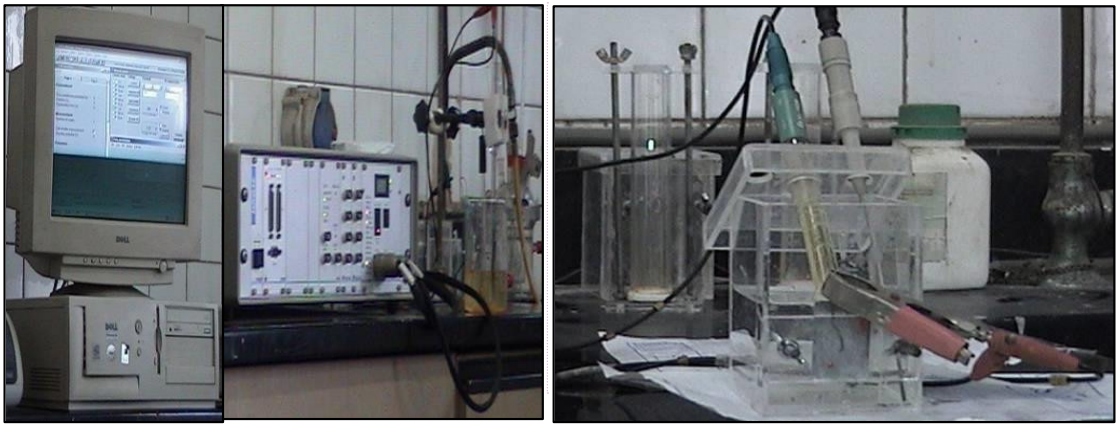

**Figure 2:** Photograph of AUTOLAP PGSTAT 30 Corrosion cell

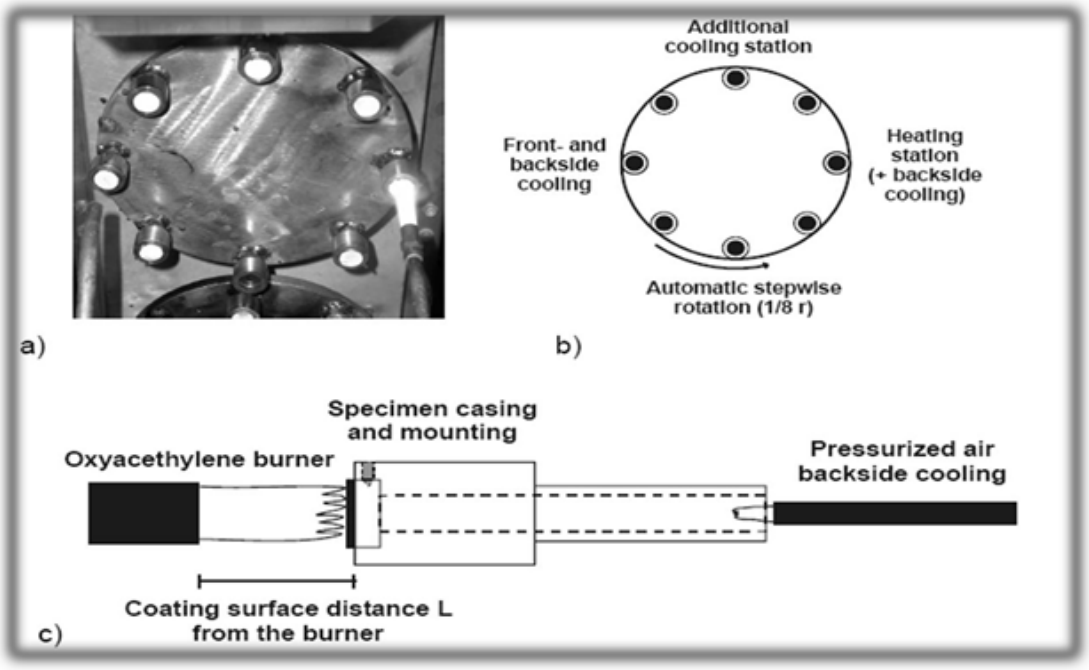


**Figure 3:** Illustration of the thermal cycling device, a) photo of the super specimen holder during test, b) position of heating and cooling stations and C) side view of the specimen mounting

| Parameter | Test |
|---|---|
| Coating burner distance (mm) | 50 |
| Coating maximum temperature C° | 1200 |
| Coating minimum temperature C° | 250 ± 50 |
| Heating time (sec) | 20 |
| Total cycle number | 500 |

**Table 1:** Thermal cycling test parameter

## Result and discussion

### Influence Of The Plasma Spray Parameter

#### On Coating Performance

The effect of plasma spray parameters on coating performance, plasma voltage versus $H_2$ - content % and Metallographic / Image analysis of sprayed Ni - Al bond coat and $ZrO_2$ – Mg O topcoat with different spray parameters are show in tables (2, 3) and Figure (4, 5), and Figure (6, 7) receptivity.

| Specimen No | Plasma gas flow rate (L/min) | | H2-content (%) | Plasma voltage (V) | Hardness $HV_3$) | Tensile bond strength (M. Pa) | Porosity (%) | Thickness (µ. m) |
|---|---|---|---|---|---|---|---|---|
| | Ar | H2 | | | | | | |
| $S_0$ | 47 | 9.5 | 20.2 | 68 | 190 | 35 | 2 | 250 |
| $S_1$ | 47 | 8.6 | 18.2 | 60 | 150 | 30 | 6 | 160 |

**Table 2:** The effect of the plasma gas on the coating performance of Ni - Al bond coat, at plasma current = 450 A, injector angle = 90°, substrate temperature = 140°C, and injection distance = 130 mm

| Specimen No | Plasma gas flow rate (L/min | | H2-content (%) | Plasma voltage (V) | Hardness $HV_3$) | Tensile bond strength (M. Pa) | Corrosion rate (m. p. y) | Porosity (%) | Thickness (µ. m) |
|---|---|---|---|---|---|---|---|---|---|
| | Ar | H2 | | | | | | | |
| $S_0$ | 47 | 13 | 27.6 | 72 | 200 | 22 | 0.0683 | 9.8 | 230 |
| $S_1$ | 47 | 0 | 0 | 27 | 115 | 12 | 0.99135 | 18.9 | 155 |

**Table 3:** The effect of the plasma gas on the coating performance of Zr. O -Mg O top coat 2 at plasma current = 630 A, injection angle = 90°, substrate temperature = 150°C, and spraying distance = 90mm

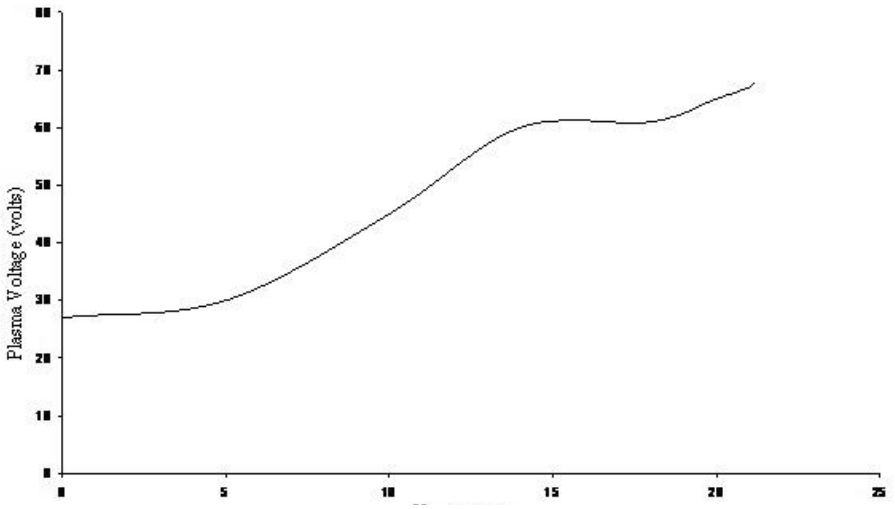


**Figure 4:** Effect of H2 - content % on plasma voltage (plasma voltage versus H2 - content %): Total flow rate = 56.5 L / min, I = 450 for Ni - Al bond coat

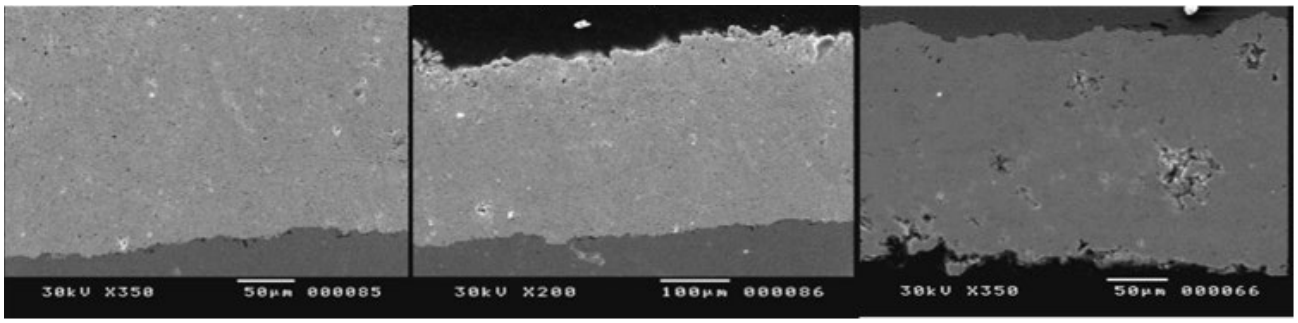


**Figure 5:** Back scattered SEM image for cross section view of (Ni- 5wt% - Al bond coat) coatings sprayed with the optimum conditions ($S_0$, Nickel - Aluminum (bon coat) coating sprayed with the optimum condition. ), with decreasing of the $H_2$ -gas flow rate ($S_1$ $H_2$ - Content 18.2% plasma voltage 60V porosity percentage 6%)

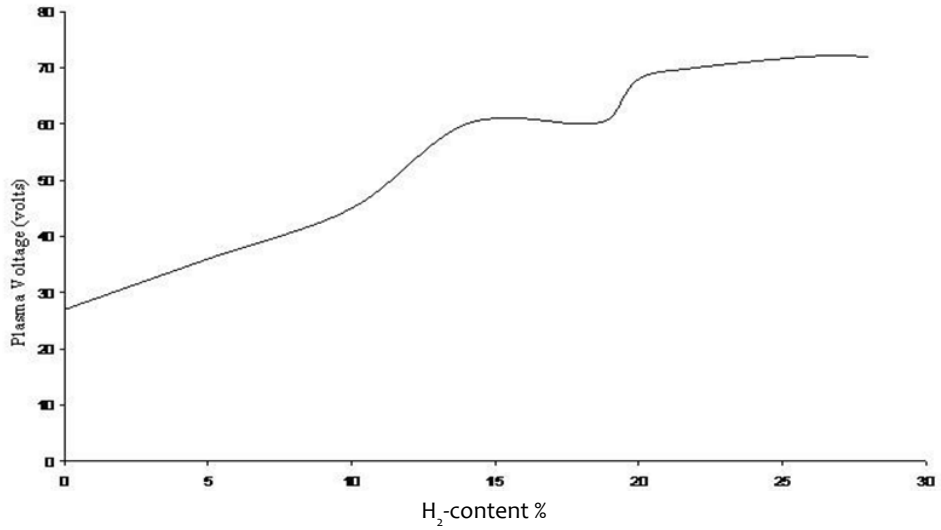


**Figure 6:** Effect of $H_2$-content % on plasma voltage, (plasma voltage versus $H_2$ -content): Total flow rate = 60 L/min, I = 630A for zirconia (top coat) coating

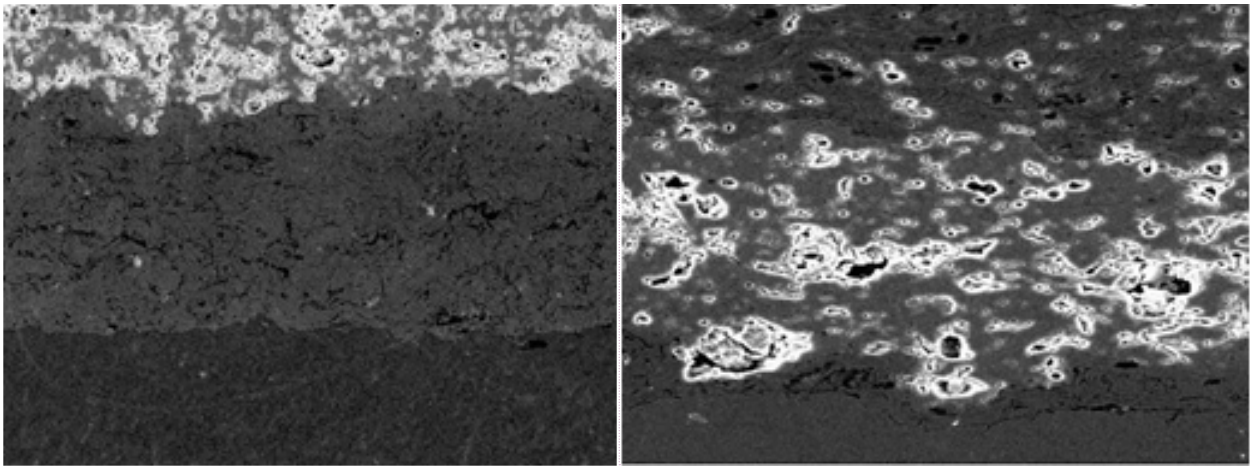

X-150 (Sub) + (Ni - Al) + ($ZrO_2$-MgO) (/So)

X - 150 ($ZrO_2$ - MgO) + (Ni-Al) Pure Ar (no H2), plasma voltages 27.6 V (/S1)

**Figure 7:** Back scattered SEM image for cross-section view of zirconia (top coat) coatings on Nickel-Aluminum (bond coat) sprayed with the optimum conditions (/So), without H2-gas flow rate (/S1)

## Advanced Processing Approaches for Producing TBCs of High Quality Performance

### Pretreatment of substrate

The average surface roughness was able to be increased from 10µm (by using shut blasting method) up to 20 µ . m (by using NTA with applying LPPS). Figure (8) and table (4) shows installation on LPPS and NTA process parameter.

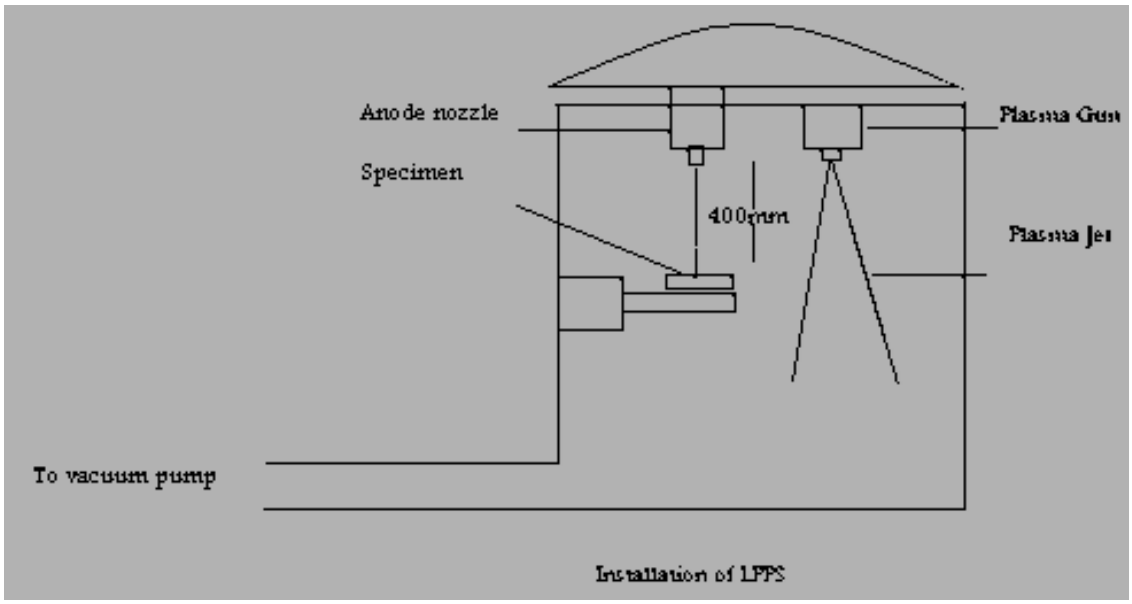


**Figure 8:** Installation of LPPS

| Plasma Generating Gas | Pressure of Plasma | Distance Between Gun and Specimen (mm) | Duration of NTA Processing (Sec) | NTA Electric Current (A) | Surface Roughness (µm) | Improved Tensile bond Strength (MPa) |
|---|---|---|---|---|---|---|
| Ar + 15 vol % $H_2$ | 25 | 500 | 0.1 - 2 | 35A | 20 ± 2 | 65 |

**Table 4:** NTA process parameter on the surface of specimens (Ni-super alloy substrate)

### Post - spray treatment procedure

#### Heat treatment

An example of the furnace annealing of T.TBCs can be illustrated in table (5).

The effect of sintering on ZrO2 - MgO top coating is illustrated in SEM micrographs, Fig (9), by remaining strings of fine pores and closed crack at splate boundaries.

| Sprayed Material Type | Furnace treatment | | | Property improved | | | | | | | |
|---|---|---|---|---|---|---|---|---|---|---|---|
| | Temperature (C°) | Time (h) | Atmosphere | Porosity (%) | | Density (gm./cc) | | Young's Modulus (G. Pa) | | Tensile bond strength on coated substrate (M Pa) | |
| | | | | Before | After | Before | After | Before | After | Before | After |
| Ni-5wt% Al bond coat sprayed on Ni-substrate | 1150 / 800 | 2 / 24 | Vacuum | ---- | ---- | 7.50 | 7.51 | 190 | 200 | 65 | 80 |
| 65 wt% ZrO2MgO plus 35wt% Ni- Al interme-diate coat sprayed on the bond coat | 800 | 4 | Air | ---- | ---- | 5.51 | 5.66 | 91 | 135 | 37 | 54 |
| ZrO2-20wt % MgO top coat sprayed on the intermediate | 1150 | 4 | Air | 9.8 | 5.8 | 4.23 | 4.48 | 62 | 69 | 33 | 48 |

**Table 5:** The effect of the Furnace treatment on the coating performance of T TBCs

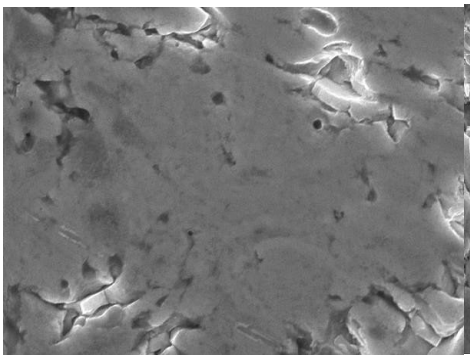

X: 2000
Annealed $ZrO_2$-MgO top coat sprayed with the optimum conditions

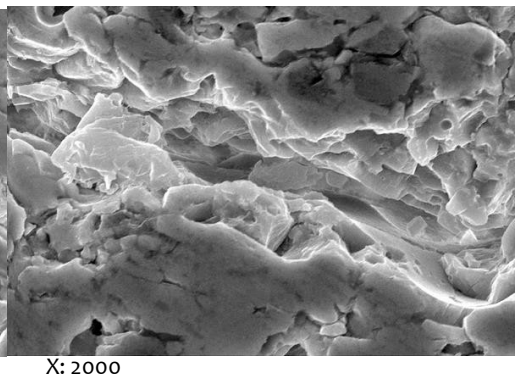

X: 2000
$ZrO_2$ - MgO top coat
Sprayed with the optimum conditions

**Figure 9:** SEM micrographs of annealed and not annealed TBCS which are thermally sprayed at the same optimum conditions illustrating the sintering of the ZrO2 - MgO top coat structure, string of the fine pores and closed cracks at splat boundaries for annealed coating

**Surface densification**

The Zr $O_2$ – Mg O coating were sealed with either Al $(OH)_2$- 85% $H_3PO_4$ solution at 300 Co for 4 hours or pulsed NAG Laser has radiation wave length of 1064 nm.

The high magnification SEM micrographs in figure (10) showed no visible reaction layer in the coating / sealant interface. But the quantitativeXRD analysis in table (6) , For $AlPO_4$ sealing showed a clear $ZrP_2O_7$ peaks with phase transition due to the following reaction.

$$ZrO_2\text{-}(MgO) + 2ALPO_4 \xrightarrow{Sealing(300°c)} ZrP_2O_7(MgO) + Al_2O_3$$

For laser sealing showed grain refining without phase transition due to the localization nature of laser:

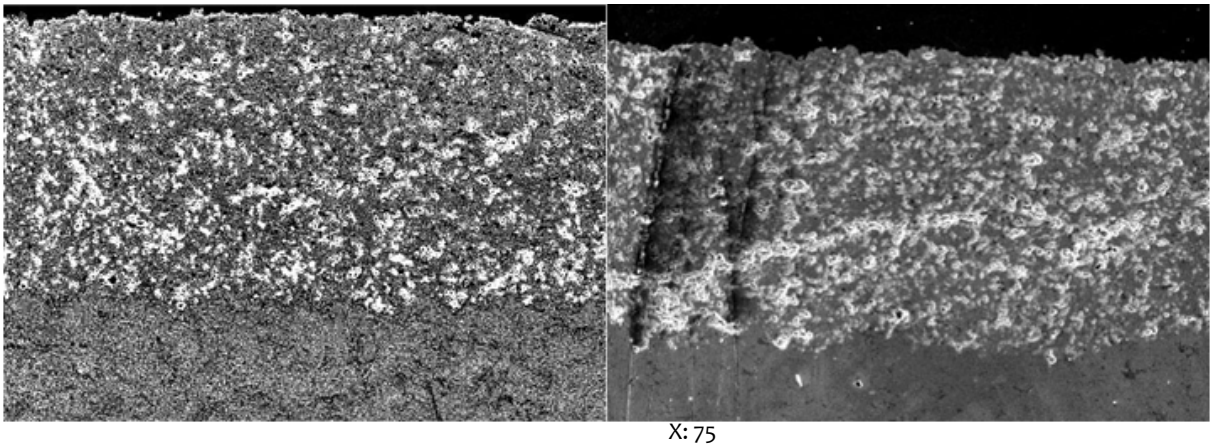

X: 75
Reference coating
(a)

X: 75
Aluminum phosphate sealed (penetration of Aluminum phosphate sealant into the ZrO2 - MgO2 top coat)
(b)

**Figure 10:** Optical micrographs of (a) reference coating, (b) modified Al PO4 coating based TTBCs

| Position of analysis | Compound wt % | | | | | Element wt % | | | | |
|---|---|---|---|---|---|---|---|---|---|---|
| | ZrO2 | MgO | $Alpo_4$ | $Zrp_2o_7$ | $Al_2o_3$ | Zr | Mg | Al | P | O |
| Outer the coating cracks | 78.2 | 21.8 | — | — | — | 60.9 | 13.1 | — | — | 25.9 |
| Inner the coating cracks | 77.9 | 21.8 | 0.05 | 0.12 | 0.13 | 60.7 | 9.3 | 2 | 1.8 | 26.2 |

**Table 6:** EDX result of Al PO4 sealed ZrO2 - MgO coatings

**Thermal expansion of thermal cycling and calculated thermal conductivity corresponding to the measured porosity**

TEC of the mixed of ceramic (65 wt % $ZrO_2$- MgO) with alloy (35 wt % Ni Al) intermediate coating was about ($12 \times 10^{-6}$ $K^{-1}$) which is close to that of substrate ($18 \times 10^{-6}$ $K^{-1}$ ), bond coat ($14.9 \times 10^{-6}$ K ) and top coat ($9.5 \times 10^{-6}$ $k^{-1}$), this lead to reduce the generation of residueal stress.

Coating failure by thermal cycles depends on the applied stress.

SEM after different cycles are presented in figure (11).

Pure Zirconia (not stabilized Zirconia) coating was damage after 280 cycles showed visible delamination and craking. Refe ence (not modified) double layer coatings was showed a horizontal and vertical crack after laser (or Al PO4) sealed ZrO2- MgO topcoat did not show any change and resisted more than 500 cycles, the coating peeled of near the bond coat after 950 cycles.

The Calculation of thethermal conductivity λ (T) corresponding to the measured porosity results are present in table (7).

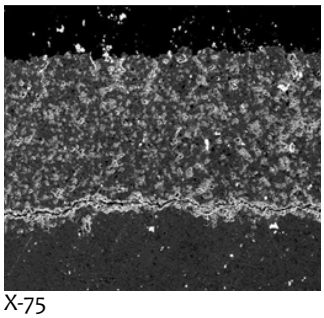

X-75
Reference coating after 500cycles (A)

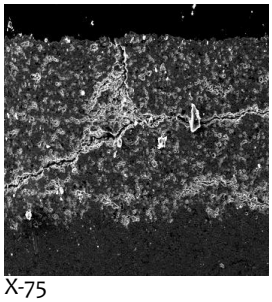

X-75
Reference coating after 400cycles (B)

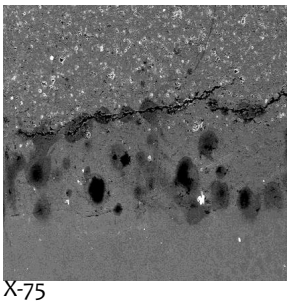

X-75
Non stabilized ZaO2 after 280 cycles (C)

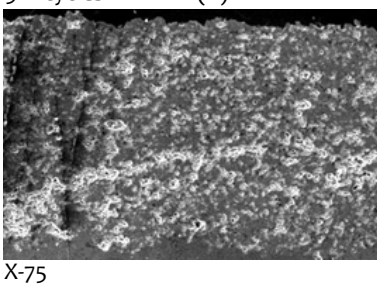

X-75
$AlPO_4$ sealed $ZrO_2$ - MgO (D)

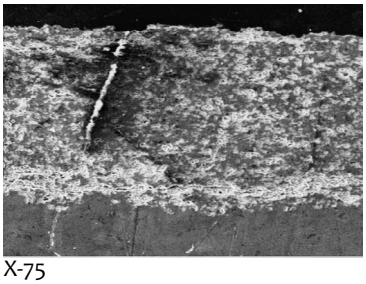

X-75
AlPO4 sealed ZrO2 - MgO after 500 cycles (E)

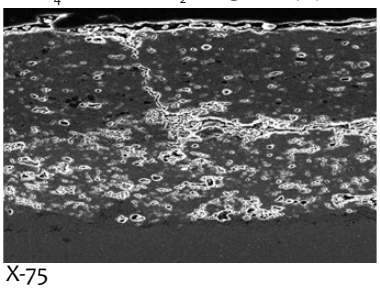

X-75
Laser sealed $ZrO_2$ – MgO (F)

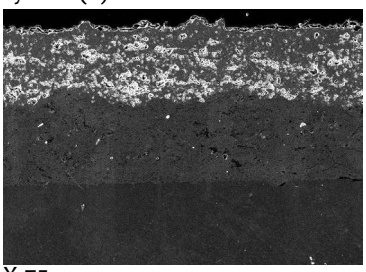

X-75
Laser sealed ZrO2 - MgO after 500 cycles (G)

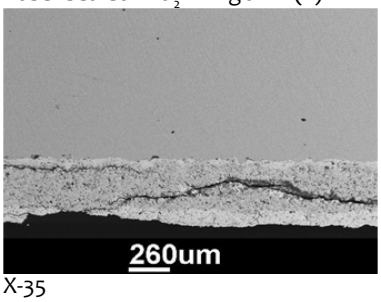


X-35
Modified coating of AlPO4 sealed ZrO2 -MgO after 950 cycles (Triple Coating) (H)

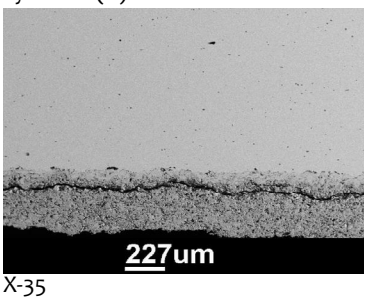


X-35
Modified coating of laser sealed ZrO2 - MgO after 950 cycles (Triple Coating) (I)

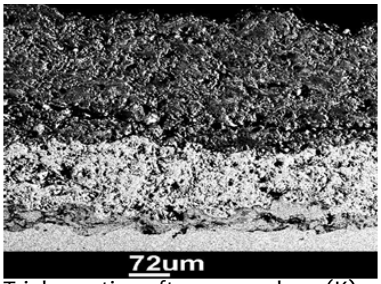


Triple coating after 500 cycles (K)

**Figure 11:** Optical microstructure (SEM) of undamaged coatings and damage coatings after 280, 400, 500 and 950 cycles

| Coating layer type deposited on Ni substrate using APS technique | Porosity (δ) % | Density (ρ) Kg/m3 | Specific heat (Cp) J/Kg/K | Thermal diffusivity $\alpha * 10^{-7}$ $m^2/S$ | Thermal Conductivity $\lambda = \rho C p \alpha$ W/mK |
|---|---|---|---|---|---|
| Ni - base - suepr allay Din (2.4631) | 0.1 | 8900 | 444<br>580<br>635<br>647 | 190<br>130<br>150<br>160 | 75<br>66<br>84.7<br>92.1 |
| Ni - 5wt % Al bond coat | 2 | 7500 | 450<br>530<br>560<br>585 | 40<br>41.5<br>43<br>34 | 9<br>10.2<br>13<br>15 |
| ZrO2 - 20 wt% MgO | 9.8 | 4280 | 614<br>640<br>657<br>660 | 2.85<br>7.5<br>7.8<br>8.85 | 0.75<br>2<br>2.2<br>2.5 |
| Aluminum phosphate sealed ZrO2 - 20 wt% MgO to coat (modified coating) | 2.9 | 4380 | 625<br>675<br>680<br>684 | 4.3<br>9.1<br>10.4<br>12.7 | 1.2<br>2.7<br>3.1<br>3.8 |
| Laser sealed ZrO2- 20 wt% MgO top coat (modified coating) | 3.9 | 4350 | 634<br>650<br>655<br>667 | 2.9<br>7.4<br>8.4<br>8.7 | 0.8<br>2.1<br>2.4<br>2.55 |

**Table 7:** Calculated thermal conductivity, λ (T) results for reference material was used in λ (T) calculations also for modified coatings corresponding to the measured porosity

**Modified corrosion resistance and corresponding Vickers Hardness investigations**

The electromagnetic parameters derived from linear polarization on experiment and the corresponding Vickers hardness for blank, reference, and modified specimens with the same spray conditions are present in table (8).

| Specimen Type | $E_{corr}$ (v) | $R_p$ ohm. $Cm^2$ *$10^3$ | $I_{corr}$ µA/Cm | Corrosion rate (mpy) |
|---|---|---|---|---|
| Ni-base super alloy substrate | -0.297 | 8.416 | 3.2906 | 0.97832 |
| ZrO2 - MgO reference coating | -0.237 | 185.8 | 0.22988 | 0.06834 |
| Aluminum - Phosphatesealed ZrO2- MgO Modified coating | -0.318 | 83.3 | 0.1802 | 0.053 |
| Laser - sealed $ZrO_2$ - MgO modified coating | -0.165 | 2899 | 0.01678 | 0.004 |

**Table 8:** The electromechanically parameters. Corrosion potential $E_{corr}$, corrosion current $I_{corr}$, polarization resistance $R_P$, and corrosion rate $C_R$ derived from linear polarization experiments and the corresponding hardness ($HV_3$) for blank specimen, reference and modified coatings with the same spray conditions

## Conclusion

Plasma spraying has great advantage over the known galvanizing process in cases where it can be used to coat electrically non conductive surface with metal.

The deviation of plasma spray parameters from the optimum condition lead to the fine microstructure coating became lower in quality i.e. increase of porosity, voids (pull - out effect), un-melted phase, and delamination.

The strengthening in phosphate sealing result from two different mechanism, chemical bonding and adhesive binding. Due to chemical reaction and formation of condensed aluminum phosphates in the structure defects of the coating.

The sealed top-coat in a few microns (50µm 100µm) were highly density and grain refined with the exception of some closed pores formed in the laser sealing process.

Phosphate sealed coating showed excellent wear resistance, 80% lower weight losses than the reference coatings.

Laser sealed coating was even more micro hardness and more abrasion resistance than the phosphate sealed coating, only a minor part of the melted top layer was worn away.

## Future work in tbcs

TBCs, need further development work, both in production technology and characterization Erosion - corrosion resistant, TBCs are needed to prevent overheating of metal part in engines and heat exchangers, for which both coating formulation and deposition methods are needed.

Thicker Zirconia coatings and more strain - tolerant coatings are needed for combustion Zones of aero gas turbine engines.

Repair of joining techniques for coating materials are always in need of further research. Some turbine blades in service have been re - coated several times, showing the importance of this aspect.

## Reference

1) P.J. Meyer and D. Hawley: in Thermal Spray Coatings: Properties, Processes and

Applications, T.F. Bernecki, ed., ASM International, Materials Park, OH, USA, 1991, p. 29-38.

2) A. Freslon, "Plasma Spraying at Controlled Temperature and atmosphere" in Thermal Spray Science and Technology, C.C. Berndt and S. Sampath, eds., ASM International, Materials park, OH, USA, 1995, p. 57 - 63.

3) T. Lewis, L. Sokol, and E. Hanna, "Optimization of Gator- gard Applied Chromium Carbide- Ni Cr Aly Composite Overlays for Maximum Solid Particle Erosion Resistance, in Thermal Spray", Advances in Coatings Technology, D.L. Houck, ed ASM International, Materials

Park, OH, USA, 1988, p. 149- 155.

4) T. Morischita, "Coatings by 250 kW Plasma Jet Spray System.' Plasma Technik 2nd Symp., S. Blum- Sandmeier, H. Eschnauer, P. Huber, and A.R. Nicoll., eds., Plasma Technik Wohlen, Wholen, CH, 1991, vol. 1, p. 137 - 45.

5) T.C. Mc Geary and J.M. Koffshey, "Engineering Applications for Flame Plating", Met. Progr., 1965, Jan., p. 80- 86.

6) M.L: Thrope and H.J. Richter, "A Pragmatic Analysis and Comparison of HVOF process", J. Thermal Spray Technol., 1992, vol. 1 (2), p. 161- 70.

7) Smith, G.D. and J.A.E. Bell, "Thermal Barrier Coating of Incoloy Alloy 909", Proceedings of the 1989 Spring TMS Meeting, las Vegas Nevada.

8) Hillery , R.V., B.H. Pilsner, R.L Mcknight, T.S. Cook and M.S. Hartle, "Thermal Barrier coating life predication Model Development. Final Report" NASA CR - 180807 (1988).

9) Miller, R.A. and C.E. Lowell "Failure Mechanisms of thermal Bareier Coatings Exposed to Elevated Temperatures", This Solid Films, 95, pp. 265- 273 (1982)

10) Miller, R.A., "Current Status of thermal Barrier Coatings- An Overview" Surface and Coatings Technology, 30, pp. 1- 11 (1987).

11) Stecura, S., "Two - layer thermal - Barrier Systems for Ni - Al - Mo Alloy and effects of Alloy Thermal Expansion on System life" Amer. Ceramic Soc. Bull., 61 (2), pp. 256- 262 (1982)

12) Novak, R.C., A. P. Matarese and R.P. Huston, "Development of Thermal Barrier coatings for Diesel Applications", Thermal Spray Technology, ASM International, pp. 273- 281 (1989).